Three-Dimensional CFD Model for a Flat Plate Photocatalytic Reactor: Degradation of TCE in a Serpentine Flow Field

Asefeh Jarandehei and Alex De Visscher
Dept. of Chemical and Petroleum Engineering and Centre for Environmental Engineering Research and Education (CEERE), University of Calgary, Schulich School of Engineering, Calgary, AB T2N 1N4, Canada

DOI 10.1002/aic.11692
Published online December 24, 2008 in Wiley InterScience (www.interscience.wiley.com).

Computational fluid dynamics (CFD) simulation was applied to a photocatalytic reactor with surface reaction for trichloroethylene (TCE) oxidation at various pollutant concentrations, and flow rates. First-order and Langmuir-Hinshelwood kinetics for TCE removal rate were considered. The results were compared with those from experiments of Demeestere et al. (Appl Catal B Environ. 2004;54:261–274) in a flat plate photocatalytic reactor with serpentine geometry. The flow regime was laminar. Through the CFD simulation, the velocity field and the concentration gradient of TCE in the reactor were studied in detail. At Reynolds numbers around 900, the laminar flow becomes unstable. Under such a condition, when flow passes the 180° sharp turns, due to formation of secondary flow and consequently vortices, there is a lot of cross-sectional mixing in the reactor. This kind of studies can help us to model the photocatalytic reactor as accurately as possible. © 2008 American Institute of Chemical Engineers *AIChE J,* 55: 312–320, 2009
Keywords: CFD, flow modeling, photocatalytic degradation, TCE, serpentine flow field

Introduction

Photocatalysis is a promising technique which utilizes semiconductors like TiO_2, ZnO, WO_3, $FeTiO_3$, and $SrTiO_3$ to carry out a photo-induced oxidation process to degrade volatile organic compounds (VOCs) into CO_2, H_2O, and completely remove NO_x and SO_x. Particularly, this technique is promising for the degradation of VOCs, in both gaseous and aqueous phase.[1] Potential applications in the gas phase include waste gas treatment,[2] indoor air pollutant abatement,[3,4] and ambient air pollutant removal.[5,6] Nowadays, due to the contribution of these compounds to environmental problems such as tropospheric ozone formation, stratospheric ozone layer depletion and global warming, photocatalytic degradation of VOCs, and development of efficient photocatalytic reactors for large-scale applications is gaining more and more interest.[7]

Kinetic studies of photocatalytic reactions at different operational conditions have been successfully conducted by many researchers,[7–11] and some of them have modeled the radiation field for various reactor configurations as well.[11–17] However, little progress has been made towards the development of a realistic hydrodynamic model for a better understanding of fluid flow properties in photocatalytic reactors. In modeling photocatalytic reactors, two simplified models, plug flow and completely mixed, have usually been applied.[7–9,11,18,19] Flow behavior of a majority of the actual reactors deviates from these two limiting conditions. The deviation may be caused by nonuniform velocity profile, velocity fluctuation due to molecular or turbulent diffusion, by short-passing and channeling of fluid, by the presence of stagnant regions of fluid caused by the reactor shape and internals, or by the recycling of fluid within the reactor as a result

Current address of A. Jarandehei: Dept. of Chemical and Biological Engineering, University of British Columbia, Vancouver, BC, Canada.
Correspondence concerning this article should be addressed to Alex De Visscher at adevissc@ucalgary.ca.

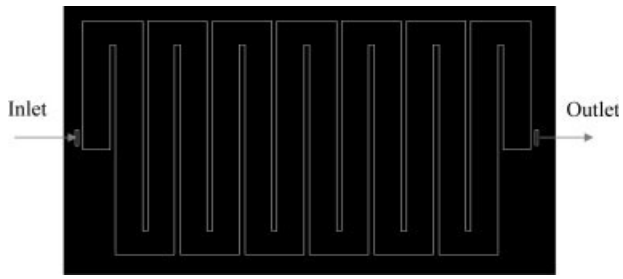

Figure 1. The top view of the 3D computational domain of the reactor.

of agitation.[20] A few researchers have developed a 2D mass balance taking into account the intrinsic kinetics, as well as mass transfer rate processes.[13,21–23] Though these models are extremely useful in providing an understanding of the fluid dynamics, these rarely can be used for engineering analysis and design. These models often work very well for well-known unit operations, but for new equipment with unknown parameters, process development would be very time consuming and difficult from laboratory to full scale. Computational flow modeling tools can accelerate the reactor engineering tasks with minimum experimentation on pilot scales and with enhanced confidence levels. For design of new equipment, engineers are increasingly using computational fluid dynamics (CFD) to analyze flow and performance. In simulation of reacting flow systems, in addition to mass and momentum equations, the mixing, transport, and production/consumption of chemical species should also be considered through species transport equations. The application of CFD in reaction engineering is well known and has been applied in many other areas of chemical engineering and chemical reaction engineering,[24] such as fluidization,[25–27] and multiphase flow systems,[28–31] and more recently, it has been utilized for simulation of photocatalytic reactors.[17,24,32–35] Pareek et al.[33] applied the CFD approach to model an annular photoreactor and analyze its performance for possible industrial wastewater treatment. A granular Eulerian approach was used to simulate the three-phase flow in a photocatalytic reactor. The model adequately described the experimental data for photodegradation of Bayer liquor. Mohseni and Taghipour[32] developed a model to predict the performance of an annular photoreactor for vinyl chloride (VC) oxidation using CFD. They applied the laminar finite rate modeling approach in which the effect of turbulence is ignored. This assumption caused about 10–20% underestimation of the degradation rate. They studied the impact of flow nonuniformities on the reactor performance and suggested some design modifications for improving reactor efficiency. Taghipour and Mohseni[35] conducted CFD modeling of a photocatalytic reactor with surface reaction for trichloroethylene (TCE) oxidation at various reactor lengths, pollutant concentrations, and flow rates in an annular reactor. They also investigated the effect of contaminated air flow thickness on the reactor performance. Though the model did not account for homogeneous reactions such as those initiated by photolysis, it predicted experimental results well except at low TCE concentrations. Castrillon et al.[24] investigated the aerodynamic behavior of a photocatalytic reactor for air treatment. They identified several design issues from simulation results and implemented some modifications to achieve uniform flow field, mass flow and contact time distributions. Sozzi and Taghipour[34] applied the CFD approach to simulate the hydrodynamics of annular UV-reactors for water treatment. In general, the CFD models showed a close agreement with the experimental data for the majority of the reactor domain and captured the influences of reactor configuration and internal reactor structures on the flow distribution. Salvado-Estivill et al.[17] performed CFD simulation of a flat plate, single-pass, and flow-through photocaralytic reactor for air purification. They studied the effect of UV irradiance (different lamp configuration), flow rate, and substrate concentration on TCE conversion. The CFD model was able to predict the experimental results reasonably.

The aim of this study is to integrate CFD with photocatalytic reaction kinetics for degradation of TCE and evaluate CFD's capability in modeling the performance of photocatalytic reactors for use in waste gas treatment; to explore the fluid flow properties and their impacts on the reactor behavior. The effect of pollutant inlet concentration and gas flow rate on the reactor efficiency has been investigated and the simulation results have been compared to data from experiments performed with a serpentine flat-plate reactor by Demeestere et al.[7]

Photocatalytic Reactor Model

Physical picture

The system under investigation is a flat-plate lab-scale photocatalytic reactor for degradation of TCE. The top view of the 3D computational domain of the reactor is shown in Figure 1. The thickness of the catalyst layer, 0.15 cm, was deducted from the actual depth of the reactor, 3 cm, and excluded from the computational domain which included the serpentine space with rectangular cross section channels containing a gaseous reaction mixture. The overall geometric dimensions of the model are outlined in Table 1. The exact geometry has been created using GAMBIT 2.3.16 (Fluent Inc) and was discretized to a sufficiently large number of control volumes or cells. The sensitivity of solution to the number of grids has been tested as well. The base grid of 710,000 cells provided a grid independent solution because the simulation results changed about 0.1% as the number of control volumes increased by a factor of 8.5.

Transport equations and kinetics

The simulation of the system was performed with a three-dimensional, steady state, single phase, laminar flow model including the photocatalytic surface reaction. The CFD simulation has been done using FLUENT 6.3.26 (Fluent Inc). In laminar flow the Navier-Stokes equations describe the mo-

Table 1. The Overall Geometric Dimensions of the Model

Parameter (m)	
Channel length	9×10^{-2}
Channel width	1×10^{-2}
Channel height	3×10^{-2}
Catalyst thickness layer	1.5×10^{-3}
Radius of curvature	1.1×10^{-2}

mentum transport. It is possible with CFD to obtain very accurate flow simulations for single phase, but care must be taken to ensure that the flow is always laminar. In the transition between laminar and turbulent flow accurate simulations are difficult. In this region, the flow can change in time between laminar and turbulent.[36] The conservation of momentum in the reactor is described by Eq. 1,

$$\frac{\partial}{\partial t}(\rho\vec{V}) + \nabla.(\rho\vec{V}\vec{V}) = -\nabla P + \nabla.\bar{\bar{\tau}} \tag{1}$$

where ρ is the density, $\vec{V}$ (m s^{-1}) is the velocity vector of fluid, P (Pa) is the pressure, and $\bar{\bar{\tau}}$ is the stress tensor. The conservation of mass is described by the continuity equation as follows,

$$\nabla.(\rho\vec{V}) = 0 \tag{2}$$

and the mass balance for each species takes the following form,

$$\frac{\partial}{\partial t}(\rho Y_i) + \nabla.(\rho\vec{V}Y_i) = -\nabla.j_i + r_i(\mathrm{MW})_i \quad i = 1, 2 \ldots n-1 \tag{3}$$

where Y_i represents mass fraction of species i, n is the number of species, j_i represents the mass diffusion flux, r_i (kg s^{-1} m^{-3}) represents the net rate of formation of a species i, and $(\mathrm{MW})_i$ is its molecular weight. As indicated below, the reaction occurs at the bottom of the reactor. Hence, $r_i = 0$ in Eq. 3, and the reaction term is incorporated in the bottom boundary condition.

The concentration of all species (reactants, by-products, and final products) in each control volume of the grid is expressed in terms of mass fraction with

$$\sum_{i=1}^{n} Y_i = 1 \tag{4}$$

As the degradation of TCE obtained by direct photolysis at the wavelength spectrum used is insignificant for all experimental conditions,[7] the only reactions considered in the simulation are the heterogeneous photocatalytic reactions occurring on the surface of TiO_2 photocatalyst. Two different kinetic models have been applied to describe this phenomenon, first-order kinetics and the Langmuir-Hinshelwood (LH) rate form.

Oxidation of TCE under dry conditions can be represented by the following reaction scheme:

$$C_2HCl_3 + 2O_2 \xrightarrow{h\nu,\mathrm{TiO_2}} 2CO_2 + Cl_2 + HCl \tag{5}$$

thus, the degradation rate of TCE is defined by first-order kinetics as follows,

$$-r_{\mathrm{TCE}} = k[C_2HCl_3] \tag{6}$$

where k is the reaction rate constant and $[C_2HCl_3]$ is the molar concentration of TCE at the catalyst layer.

The other reaction scheme taking into account the effect of dichloroacetyl chloride (DCAC) as the main intermediate product,[7,37–40] is described by Eqs. 7–9,

$$C_2HCl_3 + \frac{1}{2}O_2 \xrightarrow{n_1} C_2HCl_3O \tag{7}$$

$$C_2HCl_3O + \frac{3}{2}O_2 \xrightarrow{r_2} 2CO_2 + Cl_2 + HCl \tag{8}$$

$$C_2HCl_3 + 2O_2 \xrightarrow{r_3} 2CO_2 + Cl_2 + HCl \tag{9}$$

The direct oxidation pathway shown by Eq. 9 has been proposed based on the fact that the oxidation of a feed mixture of DCAC in air produces a different proportion of products than observed during the oxidation of TCE.[41] Furthermore, an adequate fit to the experimental results was not obtained when the direct oxidation step was ignored.[7]

The rate of each reaction step was defined by LH type rate equation:

$$r_1 = \frac{k_1[C_2HCl_3]}{1 + K_{\mathrm{TCE}}[C_2HCl_3] + K_{\mathrm{DCAC}}[C_2HCl_3O]} \tag{10}$$

$$r_2 = \frac{k_2[C_2HCl_3O]}{1 + K_{\mathrm{TCE}}[C_2HCl_3] + K_{\mathrm{DCAC}}[C_2HCl_3O]} \tag{11}$$

$$r_3 = \frac{k_3[C_2HCl_3]}{1 + K_{\mathrm{TCE}}[C_2HCl_3] + K_{\mathrm{DCAC}}[C_2HCl_3O]} \tag{12}$$

where k_1, k_2, and k_3 represent the apparent rate constants. K_{TCE} and K_{DCAC} are the adsorption constants of TCE and DCAC, respectively. The LH reaction rate as the source term has been incorporated into FLUENT through the introduction of a user defined function code written in the C language.

The rate constants k_1, k_2, and k_3 in Eqs. 10–12, as well as k in Eq. 6 are dependent on the irradiance. A power law relationship is sometimes used to express this relationship.[9,10,11,41] We assume light irradiance, and hence the rate constants, to be constant, and consider the effect of irradiance at a later stage.

In both kinetic models, the kinetic parameters have been adjusted to minimize the sum of squares of residuals between simulation and experimental results.

The kinetics assumes that the radiation field in the reactor is homogeneous. A simple radiation field calculation indicates a variation of up to 25% from the mean irradiance, resulting in a coefficient of variance of 11.5% in the irradiance. However, further calculations showed that the influence of using the average irradiance in the calculation leads to an overestimate of the average reaction rate of less than 0.2%. Hence, there is no need to consider variations of the irradiance in this system.

Boundary conditions

Uniform velocity profile and constant pressure have been defined as the inlet and outlet boundary conditions respectively. For the inlet flow, the temperature and species mass fractions have been set as well. All walls are considered to be insulated and no-slip boundary condition has been specified for the velocity at the walls. The reaction set has been assigned to the bottom surface of the reactor. Hence for the

Table 2. Model Parameters of First-Order Kinetics and LH Rate Equation

Kinetic Parameter	
k ($m^3\ m^{-2}\ s^{-1}$)	2
k_1 ($m^3\ m^{-2}\ s^{-1}$)	1.2×10^{-2}
k_2 ($m^3\ m^{-2}\ s^{-1}$)	8×10^{-4}
k_3 ($m^3\ m^{-2}\ s^{-1}$)	4×10^{-3}
K_{TCE} ($m^3\ kmol^{-1}$)	1.6×10^5
K_{DCAC} ($m^3\ kmol^{-1}$)	3.1×10^5

reactive species the vertical flux at the bottom boundary equals the reaction rate on a per area basis.

Results and Discussion

Kinetics of TCE photocatalytic oxidation

For the purpose of precisely measuring the reaction coefficients, a VOC removal process should be reaction limited to disregard the mass transfer effect.[41–43] The rate of chemical reactions is an intrinsic property of a given chemical system and is not a function of any physical process such as mixing or heat and mass transfer. It is, therefore, essential to separate the effects of physical processes from the measured experimental data to extract information about the intrinsic reaction kinetics. It is a difficult task and has some parallels with the reactor engineering activity in reverse order (measurement of reactor performance-transport processes-fluid dynamics-intrinsic kinetics).[20] Applying the CFD method, there is no longer a need to estimate the kinetic parameters based on experiments that are conducted under kinetically controlled conditions that are difficult to maintain. CFD simulation, which is taking into account the effect of mixing and mass transfer, has been used to estimate the kinetic parameters of two proposed kinetic models. Nevertheless, the uncertainties associated with CFD calculations will introduce some degree of error into the parameter estimates. The best fit values are reported in Table 2.

Velocity and concentration profiles

Simulations have been performed for different gas flow rates to investigate the fluid dynamics in the photocatalytic reactor in the range of Reynolds numbers $161 \leq Re \leq 972$. Figure 2 shows contours of velocity magnitude on the cross section of one of the reactor channels at various Reynolds numbers; the same behavior has been observed at all other channels. The contours at $Re = 161$ are not given as they are identical in shape to the contours at $Re = 215$. It is clear that at the highest Reynolds number the laminar flow became totally unstable and the threshold of instability would be the flow condition in which Re is 483. Overall as the flow passes the sharp turns, a secondary flow which is transverse to the primary flow is created and consequently causes the formation of vortices. Martin et al.[44] made a similar observation in experiments in a serpentine fuel cell with square cross section. The vectors of velocity magnitude on the centerline of one of the reactor channels are shown in Figure 3; the same

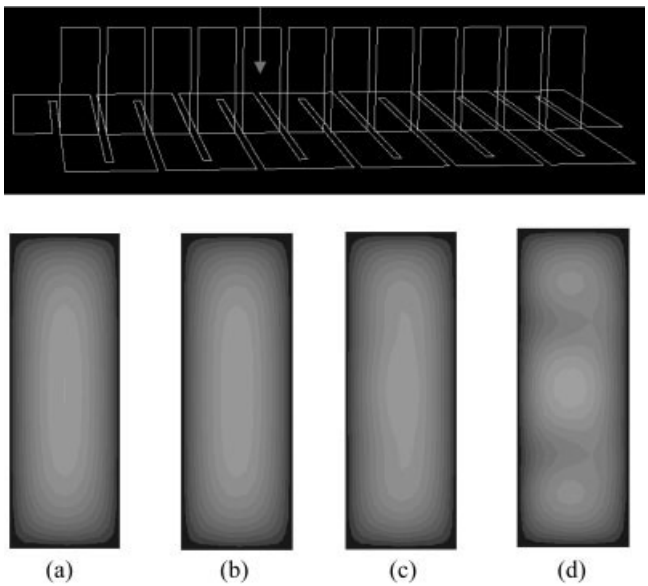

Figure 2. Contours of the velocity magnitude on the cross section of a channel of the reactor at different Reynolds numbers.

(a) $Re = 215$, (b) $Re = 323$, (c) $Re = 483$, and (d) $Re = 972$.

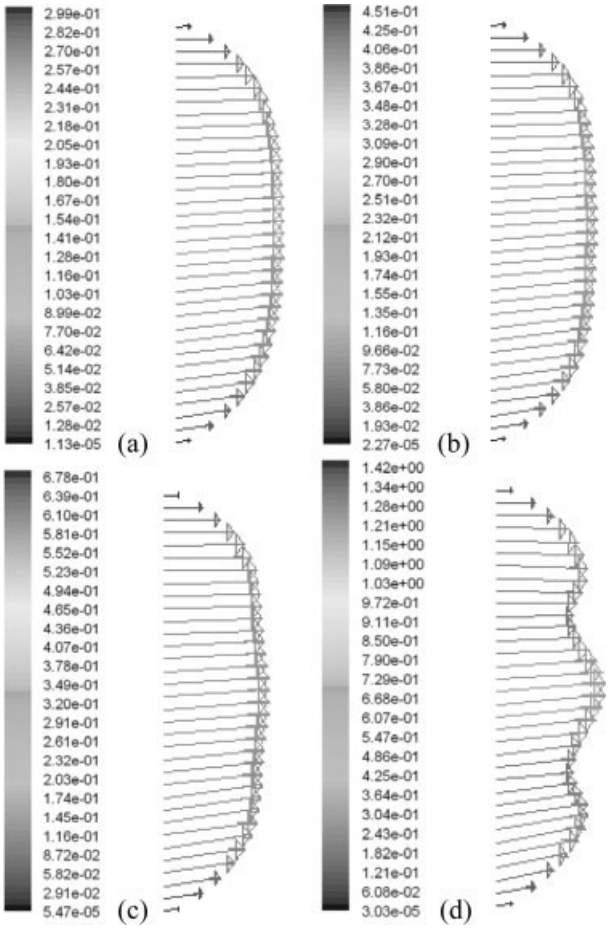

Figure 3. Vectors of velocity magnitude (m s^{-1}) on the centerline of the reactor channels at different Reynolds numbers.

(a) $Re = 215$, (b) $Re = 323$, (c) $Re = 483$, and (d) $Re = 972$.

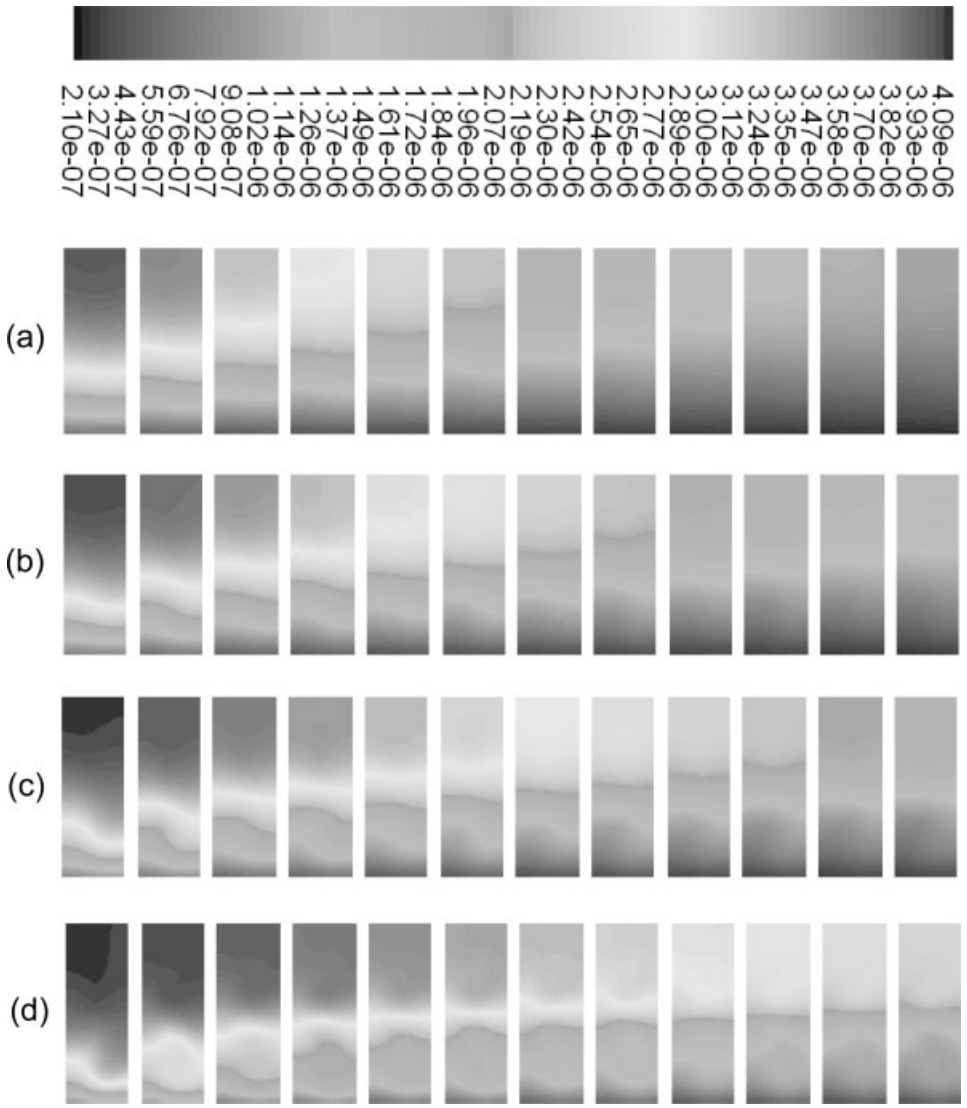

Figure 4. Contours of molar concentration of TCE (kmol m^{-3}) at an interior plane of the reactor.

(a) $Re = 215$, (b) $Re = 323$, (c) $Re = 483$, and (d) $Re = 972$. Dark shades at the top of the reactor indicate concentrations at the high end of the scale, whereas dark shades at the bottom of the reactor indicate low concentrations.

behavior has been noted at all the channels. Again, the profile at $Re = 161$ was the same in shape as the profile at $Re = 215$, and is not given. It can be observed that the velocity profile at $Re > 483$ deviates from the parabolic shape which is the characteristic of laminar flow.

Figure 4 shows the contours of molar concentration of TCE at an interior plane of the reactor. For interpretation of the gray shades with both high and low concentration indicated by dark shades, it is useful to point out that the highest concentrations are at the top of the reactor, and the lowest concentrations are at the bottom. The developing profiles are the result of reaction, advection, and diffusion of TCE in the reactor. At all Reynolds numbers the gradient in the axial direction occurs primarily as a result of advection with negligible contribution of diffusion. At the lowest Reynolds numbers, the vertical gradient is mostly due to diffusion. However, as the Reynolds number increases, extra vertical mixing can be observed because of the creation of vortices; thus vortices play an important role in mixing transport in the vertical direction. Overall the transverse gradient is not remarkable, but at highest Reynolds numbers nonuniformities can be seen. Figure 5 shows a comparison between contours of TCE concentration at highest and lowest Reynolds numbers. It is evident from the contours that the pollutant concentration changes significantly as the flow passes the channels in both cases. At the lowest Reynolds number, the contaminated stream has enough time to stay in the reactor to get decomposed. However, at the highest Reynolds number because of the high flow velocity, the polluted stream cannot be degraded efficiently. Moreover, the presence of stagnant regions at the corners of the channels may decrease the efficiency of the reactor. As is shown in Figure 6, in both cases the concentration gradient in vertical direction decreases as flow approaches the end of reactor. At the highest Reynolds number, two completely mixed regions at the top and bottom of reactor have been formed. The rate of mass transfer

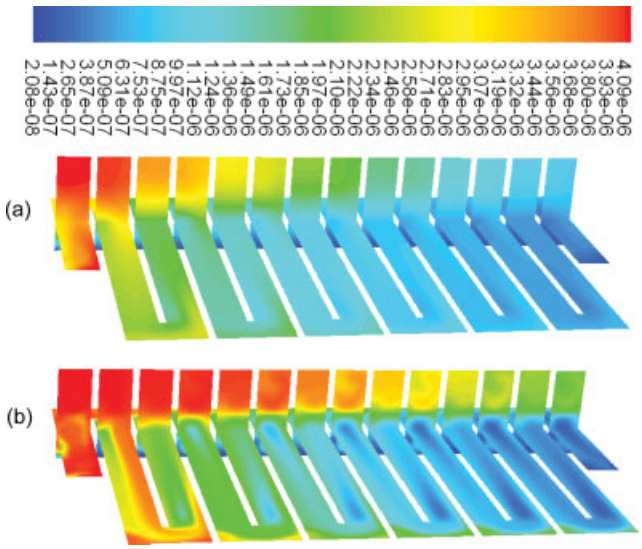

Figure 5. Contours of molar concentration of TCE (kmol m^{-3}) on the parallel plane to the top and/or bottom of the reactor.

(a) $Re = 161$ and (b) $Re = 972$.

between these two areas is low; thus, complete mixing would not be obtained even at the highest fluid velocity. In this fluid condition, although the flow regime is still laminar, a higher degree of mixing in specific regions of the reactor exists. This kind of turbulence effects is ignored by the laminar finite rate modeling approach which has been used in simulation of reaction rate and may cause some discrepancy between simulation and experimental results. Experimentally, it has been observed that the completely mixed vortices are unstable, and take turns expanding and contracting. This creates more vertical mixing than can be modeled in a steady-state CFD model.[44] We attempted to emulate this effect by increasing the mixture diffusion coefficient from 9.5×10^{-6} m^2 s^{-1} to 1.5×10^{-5} m^2 s^{-1}, as indicated in the next section.

Comparison between modeling and experimental results

Figures 7 and 8 show a comparison between CFD simulation and experimental results for prediction of removal efficiency (TCE conversion) and carbon mineralization efficiency at different gas flow rates and initial pollutant concentrations. The experimental data indicate that increasing the flow rate (or decreasing the gas residence time) reduces the

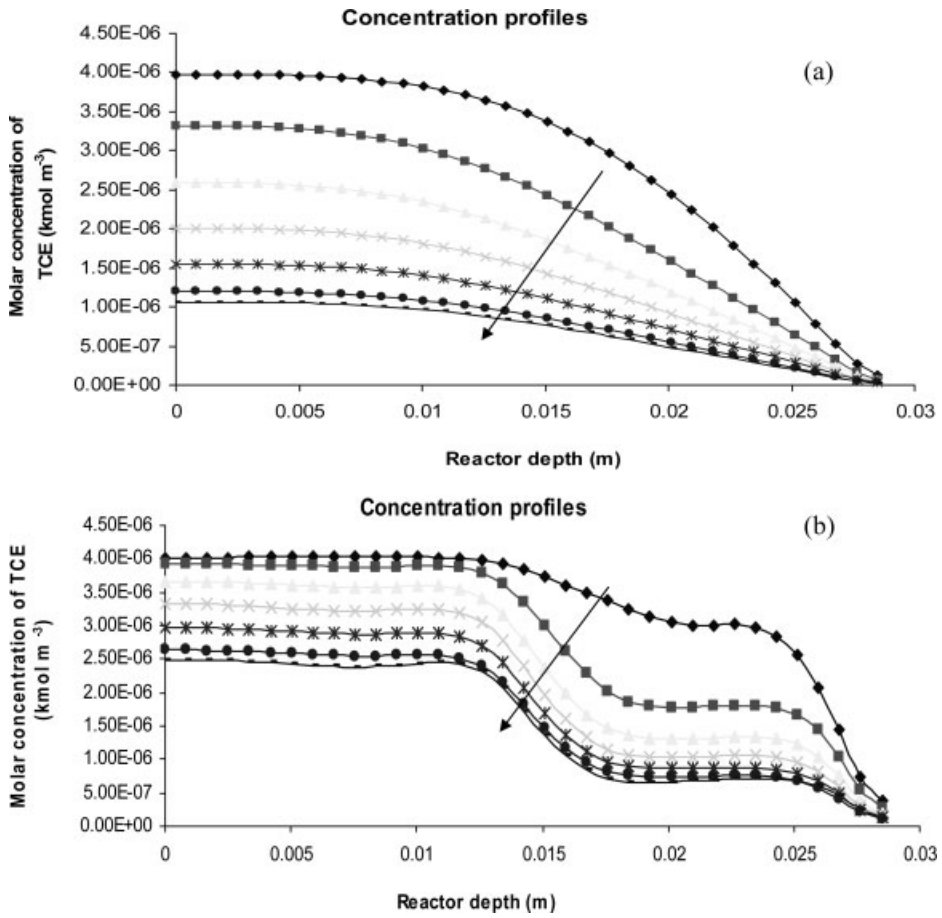

Figure 6. Concentration profiles of TCE in vertical direction at different reactor cross sections.

(a) $Re = 161$ and (b) $Re = 972$. The arrow shows the direction of flow within the reactor.

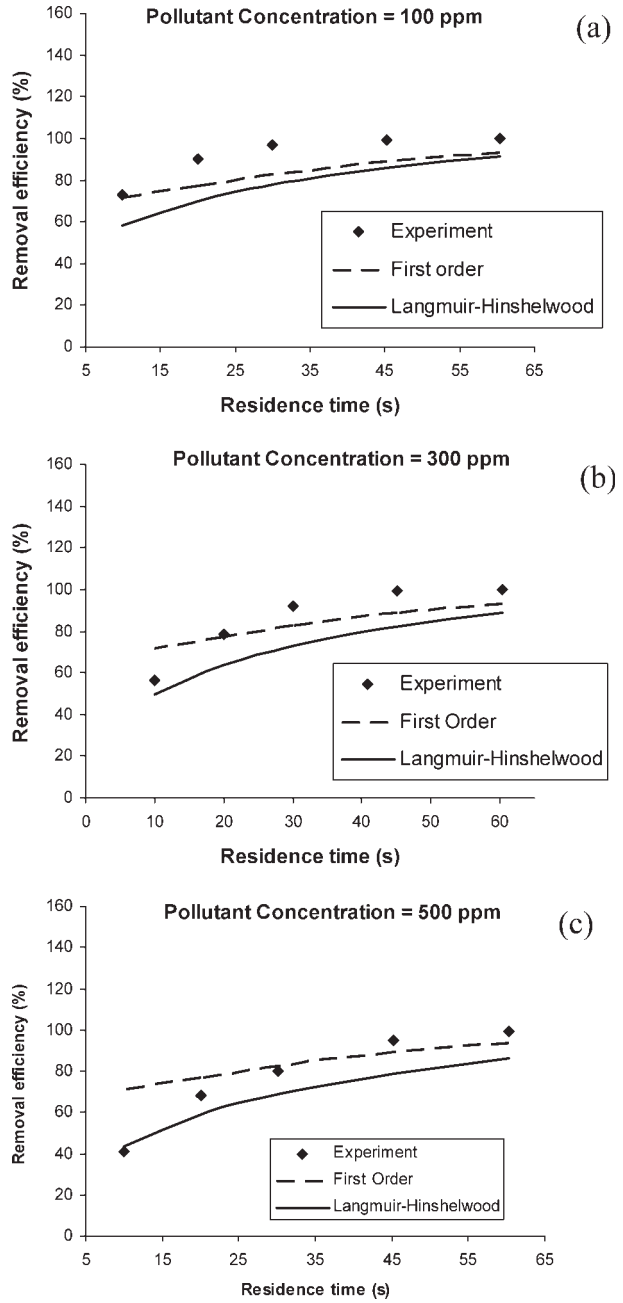

Figure 7. Modeling and experimental results of the TCE removal efficiency at different pollutant concentrations and gas flow rates.

percentage removal of TCE and consequently the production of CO_2. Both first order and LH kinetics have been able to predict the reactor behavior for degradation of TCE at different gas flow rates and results form those models are in a close agreement with experimental ones. However, the first-order kinetics greatly overestimates the amount of produced CO_2 and consequently the carbon mineralization efficiency. In the case of the first-order model, the square root of the mean square (RMS) of the relative error was 22 and 167% for TCE conversion and mineralization, respectively. For the LH model the RMS was 24 and 21%, respectively. Figures 8a–c show the experimental and modeling results for the estimation of the carbon mineralization efficiency which is lower than the removal efficiency for all experimental conditions; while the first-order kinetics could not predict this behavior, LH kinetics considering the effect of DCAC provided satisfactory estimates of the carbon mineralization efficiency. Furthermore, the first-order kinetics failed in estimating of reactor efficiency as the TCE initial concentration changed. It is evident from Figures 7a–c that the same value for TCE conversion has been predicted by the first-order kinetics at dif-

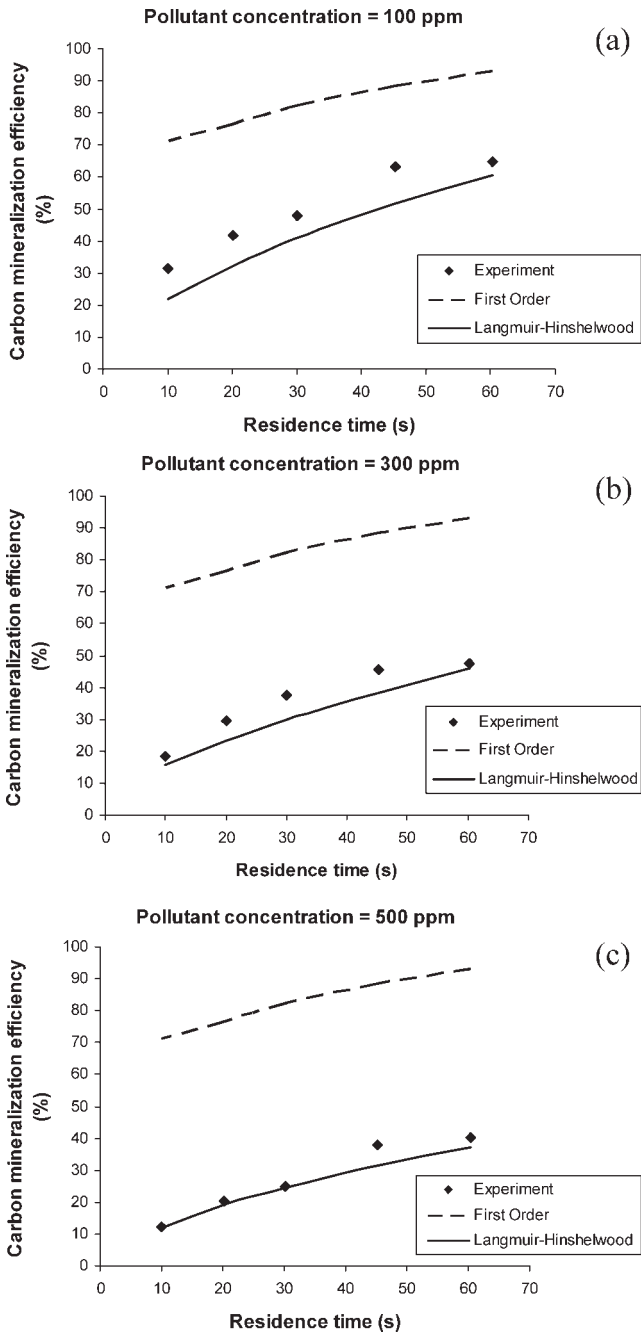

Figure 8. Modeling and experimental results of the carbon mineralization efficiency at different pollutant concentrations and gas flow rates.

ferent pollutant concentrations (100, 300, and 500 ppm) which is not consistent with actual reactor performance. The experimental data show that as the initial concentration increases, the TCE conversion declines. In spite of disadvantages of the first-order kinetic model, it is simple and easy to apply and only the reaction rate constant should be adjusted by trial and error. The other kinetic model, LH kinetics, has five tuning parameters and obviously more trial and error is needed to find the kinetic parameters providing the optimal fit to the experimental data. Although the CFD model fits the data well, it is incapable to predict the nearly complete conversion obtained at larger residence times, even by increasing the reaction rate indefinitely. Therefore, simulations were run with larger diffusion coefficient. There is uncertainty in estimation of this parameter because it changes locally as the species concentrations change. However, considering the value of 1.5×10^{-5} m^2 s^{-1} for mixture diffusion coefficient resulted in a slightly better fit for the LH model (RMS of the relative error 16% for both TCE conversion and carbon mineralization). As indicated in the previous section, this may be due to the dynamic nature of the vortices interacting with each other.

Incorporation of light irradiance in kinetic constants

The UV irradiance at the catalyst can be assumed to be constant in the experiments on which this study is based.[45] The incident irradiance was 2.86×10^{-4} meinstein g^{-1} s^{-1}.[7] The actually absorbed irradiance might be lower, about 80% of that value.[45] Hence, we assumed that the absorbed irradiance was 2.3×10^{-4} meinstein g^{-1} s^{-1}. Following Wang et al.,[46] we also assumed that the kinetic constants are proportional to the absorbed irradiance to the power of 0.61, i.e.:

$$k = k' I_a^n$$

where $n = 0.61$, and k' the kinetic constant at unit absorbed irradiance. For the first-order model, a value of $k' = 330$ m^3 m^{-2} meinstein$^{-0.61}$ $g^{0.61}$ $s^{-0.39}$ is obtained. For the LH model values of 2.0, 0.13, and 0.66 m^3 m^{-2} meinstein$^{-0.61}$ $g^{0.61}$ $s^{-0.39}$ are obtained for k'_1, k'_2, and k'_3, respectively. These values will be sensitive to the chosen value of n.

Conclusion

The behavior of a photocatalytic reactor for the degradation of TCE under various operational conditions has been investigated using the CFD method. The detailed local information of the simulated system (velocity and concentration profiles) was obtained which provided a qualitative understanding of the process to better explain the results. The detailed predicted flow field gave an accurate insight to the fluid behavior and presented information which cannot be obtained from experiments. It was found that there is a concentration gradient in the vertical direction even at high gas flow rate which has been ignored in the flow model suggested by Demeestere et al.[7] Through CFD simulation, the kinetic parameters of two different kinetic models describing photocatalytic degradation of TCE were estimated with a high degree of confidence due to consideration of the actual flow pattern in the photocatalytic reactor. The LH reaction rate form provided a better fit to the experimental results for prediction of both TCE removal efficiency and carbon mineralization efficiency.

Acknowledgments

The authors acknowledge the Natural Sciences and Engineering Research Council (NSERC) of Canada and the Canada Research Chairs program for financial support, and the Western Canada Research Grid (WestGrid) for computational resources.

Literature Cited

1. Bouzaza A, Laplanche A. Photocatalytic degradation of toluene in the gas phase: comparative study of some TiO_2 supports. *J Photochem Photobiol A Chem*. 2002;150:207–212.
2. Peral J, Domenech X, Ollis DF. Heterogeneous photocatalysis for purification, decontamination and deodorization of air. *J Chem Technol Biotechnol*. 1997;70:117–140.
3. Wan-Kuen J, Park KH. Heterogeneous photocatalysis of aromatic and chlorinated volatile organic compounds (VOCs) for non-occupational indoor air application. *Chemosphere*. 2004;57:555–565.
4. Zhao J, Yang XD. Photocatalytic oxidation for indoor air purification: a literature review. *Building Environ*. 2003;38:645–654.
5. Hou YD, Wang WC, Wu L, Ding ZX, Fu XZ. Efficient decomposition of benzene over a beta-Ga_2O_3 photocatalyst under ambient conditions. *Environ Sci Technol*. 2006;40:5799–5803.
6. Li FB, Li XZ, Ao CH, Hou MF, Lee SC. Photocatalytic conversion of NO using TiO_2-NH3 catalysts in ambient air environment. *Appl Catal B Environ*. 2004;54:275–283.
7. Demeestere K, De Visscher A, Dewulf J, Van Leeuwen M, Van Langenhove H. A new kinetic model for titanium dioxide mediated heterogeneous photocatalytic degradation of trichloroethylene in gas-phase. *Appl Catal B Environ*. 2004;54:261–274.
8. Bouzaza A, Vallet C, Laplanche A. Photocatalytic degradation of some VOCs in the gas phase using an annular flow reactor—determination of the contribution of mass transfer and chemical reaction steps in the photodegradation process. *J Photochem Photobiol A Chem*. 2006;177:212–217.
9. Ma CM, Ku Y. Photocatalytic oxidation of gaseous trichloroethylene by UV/TiO_2 process. *React Kinet Catal Lett*. 2006;89:293–301.
10. Wang W, Chiang LW, Ku Y. Decomposition of benzene in air streams by UV/TiO_2 process. *J Hazard Mater*. 2003;101:133–146.
11. Esterkin CR, Negro AC, Alfano OM, Cassano AE. Air pollution remediation in a fixed bed photocatalytic reactor coated with TiO_2. *AIChE J*. 2005;51:2298–2310.
12. Hossain MM, Raupp GB. Radiation field modeling in a photocatalytic monolith reactor. *Chem Eng Sci*. 1998;53:3771–3780.
13. Imoberdorf GE, Cassano AE, Alfano OM, Irazoqui HA. Modeling of a multiannular photocatalytic reactor for perchloroethylene degradation in air. *AIChE J*. 2006;52:1814–1823.
14. Imoberdorf GE, Cassano AE, Irazoqui HA, Alfano OM. Simulation of a multi-annular photocatalytic reactor for degradation of perchloroethylene in air: parametric analysis of radiative energy efficiencies. *Chem Eng Sci*. 2007;62:1138–1154.
15. Imoberdorf GE, Irazoqui HA, Alfano OM, Cassano AE. Scaling-up from first principles of a photocatalytic reactor for air pollution remediation. *Chem Eng Sci*. 2007;62:793–804.
16. Imoberdorf GE, Irazoqui HA, Cassano AE, Alfano OM. Photocatalytic degradation of tetrachloroethylene in gas phase on TiO_2 films: a kinetic study. *Ind Eng Chem Res*. 2005;44:6075–6085.
17. Salvado-Estivill I, Hargreaves DM, Puma GL. Evaluation of the intrinsic photocatalytic oxidation kinetics of indoor air pollutants. *Environ Sci Technol*. 2007;41:2028–2035.
18. Dibble LA, Raupp GB. Kinetics of the gas-solid heterogeneous photocatalytic oxidation of trichloroethylene by near UV illuminated titanium-dioxide. *Catal Lett*. 1990;4:345–354.
19. Ku Y, Tseng KY, Wang WY. Decomposition of gaseous acetone in an annular photoreactor coated with TiO_2 thin film. *Water Air Soil Pollut*. 2005;168:313–323.
20. Wen C-Y. *Models for Flow Systems and Chemical Reactors*. New York: Dekker, 1975.

21. Changrani RG, Raupp GB. Two-dimensional heterogeneous model for a reticulated-foam photocatalytic reactor. *AIChE J*. 2000;46:829–842.
22. Lin HF, Valsaraj KT. An optical fiber monolith reactor for photocatalytic wastewater treatment. *AIChE J*. 2006;52:2271–2280.
23. Wang W, Ku Y, Ma CM, Jeng FT. Modeling of the photocatalytic decomposition of gaseous benzene in a TiO_2 coated optical fiber photoreactor. *J Appl Electrochem*. 2005;35:709–714.
24. Castrillon SRV, Ibrahim H, de Lasa H. Flow field investigation in a photocatalytic reactor for air treatment (Photo-CREC-air). *Chem Eng Sci*. 2006;61:3343–3361.
25. Cooper S, Coronella CJ. CFD simulations of particle mixing in a binary fluidized bed. *Powder Technol*. 2005;151:27–36.
26. Grace JR, Taghipour F. Verification and validation of CFD models and dynamic similarity for fluidized beds. *Powder Technol*. 2004;139:99–110.
27. van der Hoef MA, Annaland MV, Kuipers JAM. Computational fluid dynamics for dense gas-solid fluidized beds: a multi-scale modeling strategy. *Chem Eng Sci*. 2004;59:5157–5165.
28. Jiang Y, Khadilkar MR, Al-Dahhan MH, Dudukovic AP. CFD of multiphase flow in packed-bed reactors. I. k-fluid modeling issues. *AIChE J*. 2002;48:701–715.
29. Kerdouss F, Bannari A, Proulx P. CFD modeling of gas dispersion and bubble size in a double turbine stirred tank. *Chem Eng Sci*. 2006;61:3313–3322.
30. Lamping SR, Zhang H, Allen B, Shamlou PA. Design of a prototype miniature bioreactor for high throughput automated bioprocessing. *Chem Eng Sci*. 2003;58:747–758.
31. Taha T, Cui ZF. CFD modelling of slug flow in vertical tubes. *Chem Eng Sci*. 2006;61:676–687.
32. Mohseni M, Taghipour F. Experimental and CFD analysis of photocatalytic gas phase vinyl chloride (VC) oxidation. *Chem Eng Sci*. 2004;59:1601–1609.
33. Pareek VK, Cox SJ, Brungs MP, Young B, Adesina AA. Computational fluid dynamic (CFD) simulation of a pilot-scale annular bubble column photocatalytic reactor. *Chem Eng Sci*. 2003;58:859–865.
34. Sozzi DA, Taghipour F. Computational and experimental study of annular photo-reactor hydrodynamics. *Int J Heat Fluid Flow*. 2006;27:1043–1053.
35. Taghipour F, Mohseni M. CFD simulation of UV photocatalytic reactors for air treatment. *AIChE J*. 2005;51:3039–3047.
36. Anderson B, Andersson R, Hakansson L, Mortensen M, Sudiyo R. *Computational Fluid Dynamics for Chemical Engineers*, 2nd ed. Ronnie Andersson, Goteborg, Sweden: Chalmers University, 2005.
37. Amama PB, Itoh K, Murabayashi M. Photocatalytic degradation of trichloroethylene in dry and humid atmospheres: role of gas-phase reactions. *J Mol Catal A Chem*. 2004;217:109–115.
38. Hegedus M, Dombi A. Comparative study of heterogeneous photocatalytic decomposition of tetrachloroethene and trichloroethene in the gas phase. *Appl Catal A General*. 2004;271:177–184.
39. Joung SK, Amemiya T, Murabayashi M, Itoh K. Mechanistic studies of the photocatalytic oxidation of trichloroethylene with visible-light-driven N-doped TiO_2 photocatalysts. *Chem A Eur J*. 2006;12:5526–5534.
40. Rodrigues S, Ranjit KT, Uma S, Martyanov IN, Klabunde KJ. Visible-light photooxidation of trichloroethylene by Cr-Al-MCM-41. *J Catal*. 2005;230:158–165.
41. Jacoby WA, Blake DM, Noble RD, Koval CA. Kinetics of the oxidation of trichloroethylene in air via heterogeneous photocatalysis. *J Catal*. 1995;157:87–96.
42. Mohseni M, David A. Gas phase vinyl chloride (VC) oxidation using TiO_2-based photocatalysis. *Appl Catal B Environ*. 2003;46:219–228.
43. Yamazaki S, Tanaka S, Tsukamoto H. Kinetic studies of oxidation of ethylene over a TiO_2 photocatalyst. *J Photochem Photobiol A Chem*. 1999;121:55–61.
44. Martin J, Oshkai P, Djilali N. Flow structures in a U-shaped fuel cell flow channel: quantitative visualization using particle image velocimetry. *J Fuel Cell Sci Tech*. 2005;2:70–80.
45. Jarandehei A, Karimi Golpayegani M, De Visscher A. Kinetic modeling of photocatalytic degradation reactions: effect of charge trapping. *Appl Catal B Environ*. 2008;84:65–74; doi:10.1016/j.apcatb. 2008.03.006.
46. Wang KH, Tsai HH, Hsieh YH. A study of photocatalytic degradation of trichloroethylene in vapor phase on TiO_2 photocatalyst. *Chemosphere* 1998;36:2763–2773.

Manuscript received Feb. 4, 2008, and revision received Sept. 13, 2008.